JOURNAL OF GEOPHYSICAL RESEARCH, VOL. 98, NO. E10, PAGES 18,803–18,811, OCTOBER 25, 1993

# Thermal Profiles in the Auroral Regions of Jupiter

PIERRE DROSSART AND BRUNO BÉZARD

*Centre National de la Recherche Scientifique, Départment Spatial, Observatoire de Paris-Meudon, France*

SUSHIL K. ATREYA AND JAMES BISHOP

*Deptartment of Atmospheric, Oceanic and Space Sciences, University of Michigan, Ann Arbor*

J. H. WAITE, JR., AND D. BOICE

*Southwest Research Institute, San Antonio, Texas*

The temperature structure within the northern auroral region of Jupiter is studied by reanalyzing the Voyager 1/infrared interferometer and radiometer spectrometer (IRIS) spectra. The total measured excess infrared auroral zone emission (averaged over the IRIS field of view) in the hydrocarbon bands between 7 and 13 μm is found to be about 208 ergs $cm^{-2}$ $s^{-1}$ over an area of about $2 \times 10^{18}$ $cm^2$ with a resulting power output of $4 \times 10^{13}$ W. In comparison, the total energy deposition by magnetospheric charged particles has been estimated on the basis of UV observations to range between $1 \times 10^{13}$ and $4 \times 10^{13}$ W over a comparable area. The large amount of radiated energy observed in the infrared may imply an additional heat source in the auroral regions (possibly Joule heating). A new set of thermal profiles of Jupiter's high-latitude upper atmosphere has also been derived. These profiles have a large temperature enhancement in the upper stratosphere and are constrained to reproduce the $CH_4$ emission at 7.7 μm. The emission in the other hydrocarbon bands ($C_2H_2$ and $C_2H_6$) is found to depend on the depth to which the temperature enhancement extends, which further constrains the thermal profiles. This study shows that a large temperature enhancement in the upper stratosphere and lower thermosphere can explain the observed excess hydrocarbon emission bands; thus smaller variations in hydrocarbon abundances (between the high latitudes and the equatorial and middle latitudes) are required than has been assumed in previous models.

## INTRODUCTION

Since the discovery of a thermal anomaly in Jupiter's auroral regions [*Caldwell et al.*, 1980], enhanced hydrocarbon emissions have been observed by various authors, generally around the same System III longitudes. From a reanalysis of Voyager/infrared interferometer and radiometer spectrometer (IRIS) spectra, *Kim et al.* [1985] showed that an enhanced infrared auroral emission is also observed in $C_2H_2$, $C_2H_6$, $C_2H_4$, and probably other hydrocarbons. Ground-based observations at high spectral resolution also showed a large enhancement in the $C_2H_2$ emission [*Drossart et al.*, 1986], associated with a smaller (if any) enhancement in $C_2H_6$ emission [*Drossart et al.*, 1985; *Kostiuk et al.*, 1987]. To explain these emissions, it was usually assumed that a combination of temperature increase and modified abundances of methane photochemical products is at work within the auroral regions. Assuming an isothermal structure for the high stratosphere, *Kim et al.* [1985] derived thermal profiles consistent with the $CH_4$ emission, with a temperature enhancement of the order of 30 K in the 1-mbar range. *Halthore et al.* [1988] modeled the thermal structure of the auroral hot spot as a layer of constant temperature to interpret the thermal properties of the auroral hot spot. With such thermal profiles, it is necessary to assume an increased abundance of $C_2H_2$, and a decreased abundance of $C_2H_6$, to explain the observed IRIS spectra. However, it is well known that the temperature retrieval is not well constrained in the upper part of the atmosphere [*Wallace*, 1976]; and as pointed out by *Drossart et al.* [1986], the $C_2H_2$ emission can be explained as the signature of either a temperature enhancement or an abundance enhancement. The objective in this paper is to incorporate new information on temperatures in the upper atmosphere derived from the $H_3^+$ emission [*Drossart et al.*, 1989; *Maillard et al.*, 1990; *Kim et al.*, 1992] to develop modified thermal profiles of Jupiter's high-latitude upper atmosphere in an effort to account for the excess infrared emissions.

## VOYAGER/IRIS OBSERVATIONS

Two sample IRIS spectra [*Hanel et al.*, 1979] are shown on Figure 1. The first one is within the northern auroral hot spot (54.5° ≤ latitude ≤ 62°, 180° ≤ $\lambda_{III}$ ≤ 200°; 1.7 ≤ $\mu$ ≤ 2.1; 29 spectra, FDSC numbers 16452.53–16453.07 and 16453.12–16453.25); and the second one is outside the hot spot, in the same latitude range but outside the spot longitudes ($\mu$ = 2.6, 53 spectra). The magnitude of the enhancement in the hydrocarbon emissions can be calculated from the difference between these two spectra (Figure 2). The excess enhancement is most noticeable in the strong Q branches of $CH_4$ and $C_2H_2$. The total emission for $C_2H_2$ is assumed to be twice the Q branch emission, since the total intensity of the P and R branches is equal to that of the Q branch alone, to a good approximation. For $CH_4$, where the intensities of the P, R, and Q branches are equal, the same method can be applied by measuring the Q branch emission, and multiplying it by a factor of 3.

To calculate the emission integrated over $2\pi$ sr, an assumption must be made about the angular variation of the emission. Voyager observations in the auroral hot spot were recorded at about 60° emission angle and at a distance of about $2.6 \times 10^6$ km; and the projected field of view (≈23,000 km in latitude and 11,500 km in longitude) was larger than the size of the auroral hot spot (≈9,000 km in latitude, and 25,000 km in longitude) defined by ground-based observations [*Caldwell et al.*, 1988]. This implies a filling factor of 0.4; the filling factor may even be smaller because the



Paper number 93JE01801.
0148-0227/93/93JE-01801$05.00

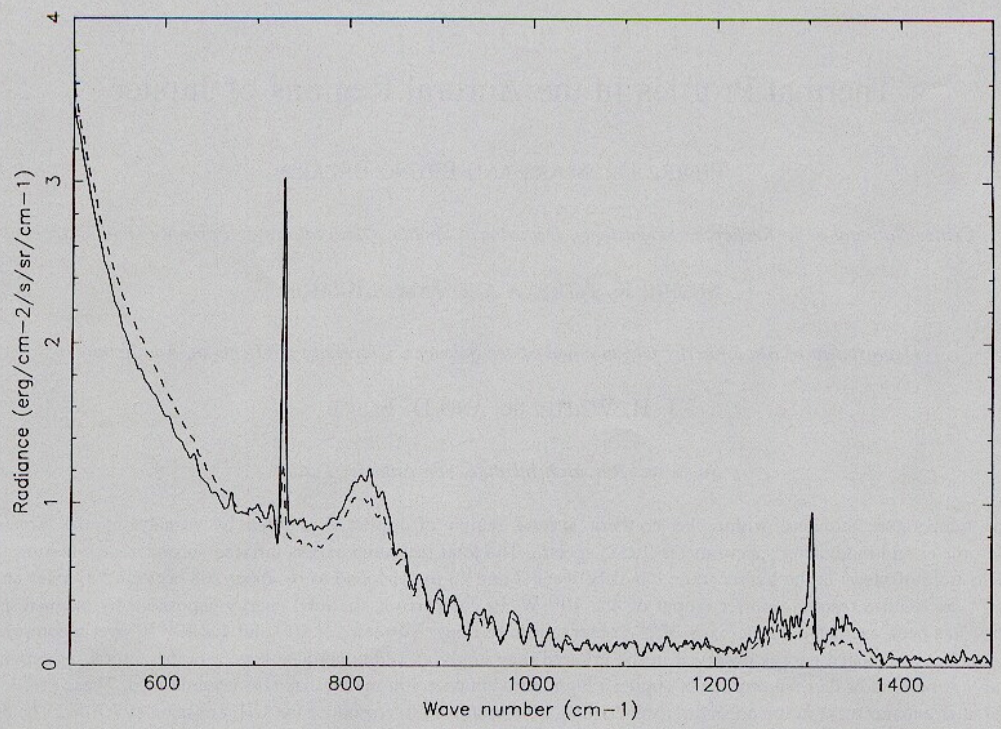


Fig. 1. Voyager/IRIS spectra. Solid line, selection of 29 spectra taken at latitudes $54.5° \leq \theta \leq 62°$ and longitudes $180° \leq \lambda_{III} \leq 200°$, which correspond to the auroral hot spot; average air mass $\mu = 1.9$. Dashed line, selection of 53 spectra at the same latitudes, but at longitudes outside the hot spot; average air mass $\mu = 2.6$.

estimate of the size of the auroral hot spot was limited in this reference (at least in latitude) by the size of the aperture (2 arc sec).

We calculate the integrated excess emission for two extreme cases.(1). Optically thin emission: in this case, $I_{60}$ being the radiance observed by the instrument at a 60° emission angle, the integrated flux will simply be $F = 2\pi I_{60}$.(2). Optically thick emission: in this case, the emission originates from the $t \approx 1$ level. If the size of the auroral hot spot is smaller than the aperture, the filling factor of the emitting region is $f_\theta = f_0 \cos\theta$, and the spectral radiance for the excess emission, at emission angle $\theta$, is given by $I_\theta = I_\theta f_\theta / f_0 = I_0 / \cos\theta$, where $I_0$ is the radiance observed at nadir. For $\theta = 60°$, the integrated flux is thus $F = \pi I_0$, and is again equal to $2\pi I_{60}$. If the

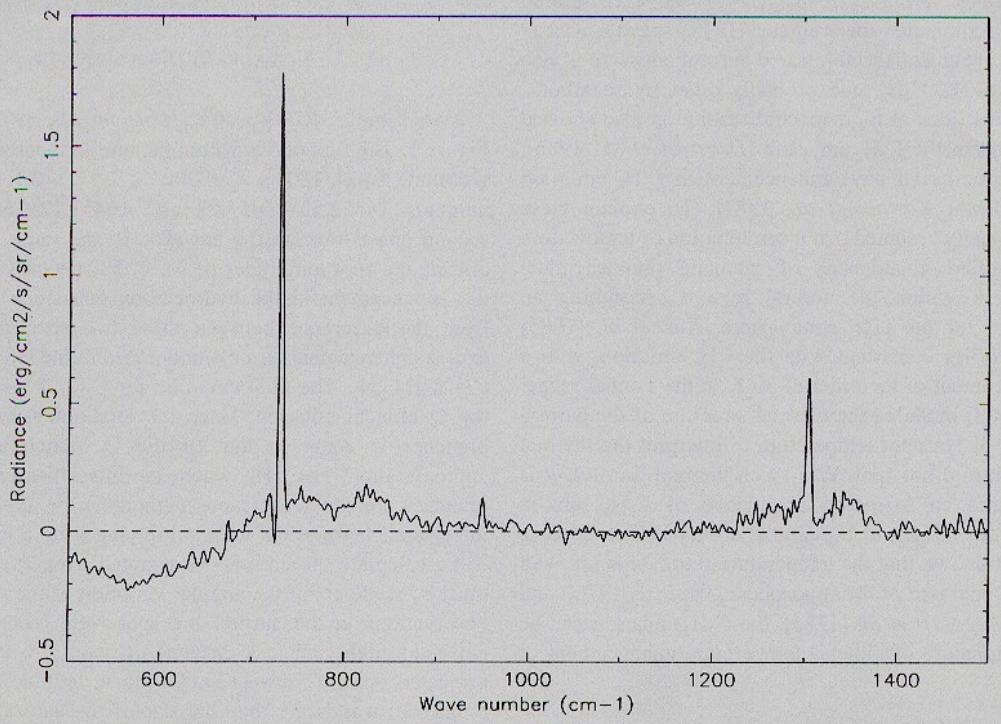


Fig. 2. Difference between the two spectra shown in Figure 1. Despite the air mass factor, which may account for the difference in the tropospheric continuum, the difference between the auroral/nonauroral spectra gives directly the auroral emission of hydrocarbons, if optically thin emission is assumed.

size of the auroral hot spot is not smaller than the aperture, the filling factor of the emitting region with be $f_\theta$ with $f_0 \cos\theta \le f_\theta \le f_0$, and the excess flux will be $\pi I_{60} \le F \le 2\pi I_{60}$.

Thus, in any case, the derived flux does not depend by more than a factor of 2 on the assumptions concerning the angular dependence of the emission.

The main error in these calculations is due to the continuum subtraction in the difference spectrum. Some difference in the continuum level is observed between the two selections below 700 $cm^{-1}$, due to the difference in the average emission angles, and possibly in the tropospheric temperatures and cloud structure. Below 900 $cm^{-1}$, this variation could affect the integration of the spectral radiance over wavenumber in the $C_2H_2$ and $C_2H_6$ bands. The estimate of the $C_2H_6$ excess emission is much less accurate than for $CH_4$ and $C_2H_2$ because the broadband emission feature of $C_2H_6$ is superposed on a significant continuum and is thus sensitive to variations in this continuum between the two selections. To correct as far as possible for effects due to the different geometry of the auroral and nonauroral spectra, a synthetic calculation has been performed with both emission angles. The emission angle effect is therefore evaluated directly and is found to be about 5% in the wavenumber interval over which the integration is performed. Another source of error in the case of the $C_2H_6$ measurement is the possibility of stratospheric temperature variations. Due to the sensitivity of the emission to the temperature (a variation of 1 K for the temperature giving rise to a variation of 4% for the flux), this effect could be quite important. In view of these effects, the $C_2H_6$ excess emission derived from the IRIS spectra could have an uncertainty of as much as 50%. Other reports of $C_2H_6$ emission variations based on high spectral resolution observations show that $C_2H_6$ has less of a variation than $C_2H_2$ [*Kostiuk et al.*, 1989]. Direct high spectral resolution observations of both $C_2H_2$ and $C_2H_6$ indicate that the variation in individual lines of $C_2H_6$ is less than 10%, compared to 100% for $C_2H_2$ [*Drossart et al.*, 1985].

The results of the integrated excess emission calculations, which correspond to an average over the global IRIS field of view, are $I(CH_4) = 93 \pm 9$ ergs $cm^{-2}$ $s^{-1}$; $I(C_2H_2) = 86 \pm 5$ ergs $cm^{-2}$ $s^{-1}$; $I(C_2H_6) = 26 \pm 13$ ergs $cm^{-2}$ $s^{-1}$; $I(C_2H_4) = 3 \pm 1$ ergs $cm^{-2}$ $s^{-1}$. The total enhancement is $208 \pm 15$ ergs $cm^{-2}$ $s^{-1}$.

## RADIATIVE TRANSFER MODEL

Assuming that the hydrocarbon auroral emissions originate in optically thin layers, we used a simple radiative transfer model to investigate the effects of temperature and species abundance on the auroral infrared emissions. The total emission within $2\pi$ sr in the $\nu_4$ band of $CH_4$ can be written as

$$I_{CH_4} = N^*_{CH_4} hc\sigma_{CH_4} A_{CH_4}/2 \qquad (1)$$

Similar expressions can be written for the other hydrocarbons, with the constants given in Table 1. $N^*_{CH4}$ is the integrated column density of $C_2H_6$ in the $\nu_4 = 1$ vibrational level, $\sigma_{CH4}$ wavenumber at band center, and $A_{CH4}$ the Einstein coefficient for the vibrational transition. Assuming local thermodynamic equilibrium (LTE), we can calculate the integrated column density as follows:

$$N^*_{CH_4}(z) = \omega_1 \int_z^{+\infty} \frac{\exp(-E^*/kT)}{Q_v(T)} N_{CH_4}(z)dz \qquad (2)$$

with $\omega_1$, ($\omega_0$) the degeneracy of the upper (lower) levels, $E^*$ the energy of the upper level of the transition, and $Q_v(T)$ the vibrational part of the partition function. The Einstein coefficient $A$ (in $s^{-1}$) is related to the band strength $S$ (in cm/molecule) by

$$A = \frac{\omega_0}{\omega_1} 8\pi\sigma^2 cS \qquad (3)$$

TABLE 1. Spectroscopic Parameters of the Hydrocarbons

| Mol. | Band | Wave#, $cm^{-1}$ | Degen. | Einstein coeff., $s^{-1}$ | Band strength $cm^{-2}$ $amagat^{-1}$ |
|---|---|---|---|---|---|
| $CH_4$ | $\nu_4$ | 1306 | 3 | 2.5 | 114 |
| $C_2H_2$ | $\nu_5$ | 729 | 2 | 5 | 535 |
| $C_2H_6$ | $\nu_9$ | 820 | 2 | 0.32 | 13 |
| $C_2H_4$ | $\nu_7$ | 949 | 1 | 8.5 | 410 |

The coefficients of this table have been calculated from the GEISA data bank [*Husson et al.*, 1986].

The validity of the LTE approximation has been checked for the $\nu_4$ band of $CH_4$, using a cooling-to-space approximation [*Houghton*, 1986]. We employed the $CH_4$ collisional relaxation time given in (19) of *Appleby* [1990]. We found that by using a nominal $CH_4$ vertical profile (see below) significant departure from LTE is limited to pressure levels less than 1 μbar. More precisely, the ratio of the source function to the Planck function reaches 0.5 at the 0.5-μbar level. Non-LTE effects slightly affect the calculated $\nu_4$ emission in the auroral hot spot (by about 5%) and have been included in the synthetic spectra calculations below.

In this formulation, we have neglected induced emission (as opposed to spontaneous emission). Inclusion of induced emission would simply replace the Boltzmann factor in the expression of $N^*$ by $1/(\exp(E^*/kT)-1)$, which has an effect of only a few percent for the temperatures and wavenumbers that are used here. The model allows a fast computation of the total energy emitted in each vibrational band of the hydrocarbons. The column density in the upper state above a given altitude $z$ can therefore be calculated for a given distribution of temperature and abundance without any further assumption.

Figure 3 shows the profiles of hydrocarbons used in our calculations. We refer to these profiles in the following as the "nominal model." These profiles represent results of a photochemical model that best describes Voyager UVS observations of the hydrocarbons and the structure of vertical mixing in Jupiter's equatorial middle and upper atmosphere [*Atreya et al.*, 1981]. Models used in this paper include minor changes in chemistry [*Bishop et al.*, 1992], spacecraft attitude information and the variation of eddy diffusion coefficient with atmospheric density, but are still constrained by the UVS occultation measurements.

The assumption of an optically thin emission layer implies a maximum pressure to which this model can be applied. We calculate the probability $p(z)$ that a photon, emitted at an altitude $z$, will be reabsorbed in the atmosphere as follows:

$$p(z) = 2\frac{1}{S}\int \alpha_\sigma^2 d\sigma \times N_0(z) \qquad (4)$$

where $\alpha_\sigma$ is the absorption cross section at the wavenumber $\sigma$, $S$ is the band strength, and $N_0$ is the particle column density. Our model is valid under the condition $p \le 1$, which is roughly equivalent to

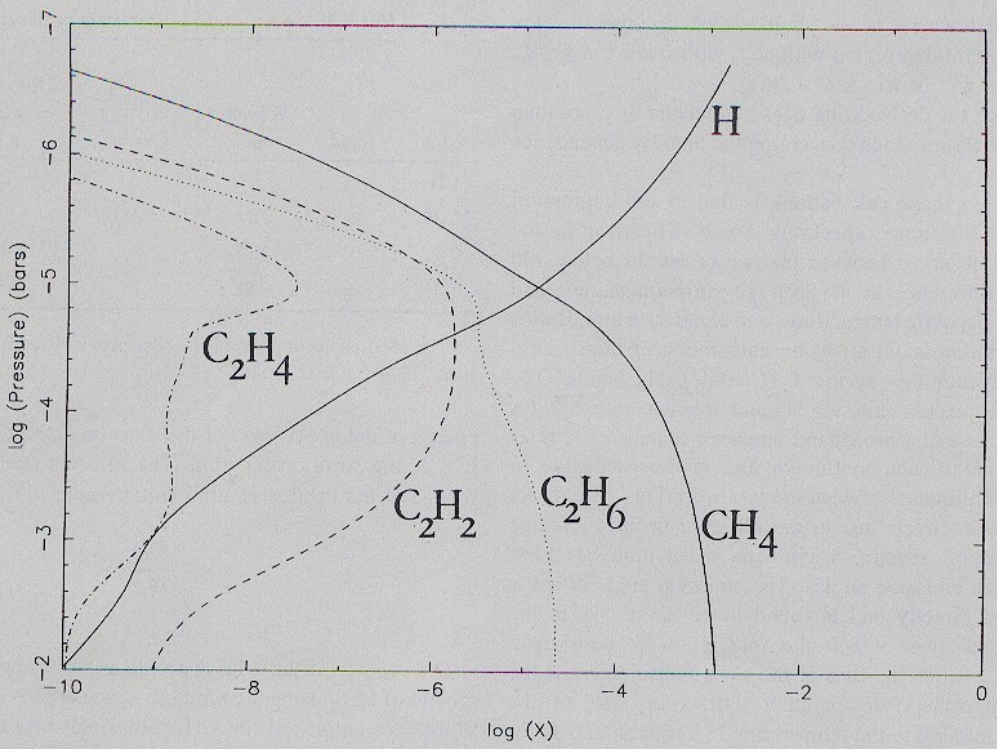


Fig. 3. Hydrocarbon vertical profiles. Using the standard conditions of the Jovian atmosphere, and an eddy diffusion coefficient of $10^6$ cm$^2$ s$^{-1}$ at the homopause, a photochemical model gives the plotted vertical variations of hydrocarbons ($CH_4$, $C_2H_2$, $C_2H_6$, $C_2H_4$).

the condition of low optical depth, although a little more restrictive. For the hydrocarbon profiles that we have selected, the optically thin condition ($p \leq 0.5$) implies $P \leq 40$ μbars for $C_2H_2$, $P \leq 50$ μbars for $CH_4$, and $P \leq 2$ mbars for $C_2H_6$.

The high intensity of the acetylene $\nu_5$ band, combined with a much lower number of lines within the band (due to the linearity of this molecule) explains why $C_2H_2$ lines become saturated at a much higher altitude than $C_2H_6$, and at an altitude comparable to that at which the $CH_4$ becomes saturated, despite its lower abundance. Therefore, the model presented here will be valid down to pressures of 20-40 μbars.

## THE THERMAL PROFILES

Emission intensity is dependent upon both the vertical distribution of the hydrocarbon species and the temperature. Thus we have used a $CH_4$ vertical distribution from the nominal hydrocarbon model to calculate a class of auroral thermal profiles, adapting each profile to fit the excess auroral $CH_4$ emission. We first derived a nominal thermal profile from the best fit of the $\nu_4$ band of $CH_4$ in the nonauroral IRIS spectrum. This profile is used at low altitudes as a lower boundary condition for the hot spot profiles. In the high-altitude range, a simple profile with a constant lapse rate is used, simulating the heating that results from the auroral processes. Then, for every given lapse rate $dT/dz$, the pressure at which the profile is connected to the nonauroral one, $P_s$, is calculated, so that the excess of column density in the $CH_4$ upper state population, compared to the nominal case, yields the observed excess emission. For large values of the lapse rate, it is clear that $P_s$ is uniquely determined. The calculated thermal profiles are shown in Figure 4.

In calculating the thermal profiles, we have taken the thermal vertical expansion of the atmosphere due to the scale height variation with temperature into account, assuming that the relative abundances of hydrocarbons remain constant with pressure, which is correct to first order. The fast calculations using the optically thin model allow us to compute the total emission within the $CH_4$-$\nu_4$ band for a given profile and to adjust it to the observed IRIS emission.

The high temperatures found in these profiles above 1 μbar (Figure 4) are not unrealistic, when compared to the high temperatures found in $H_2$ quadrupole lines [*Kim et al.*, 1990] and in the $H_3^+$ emissions [*Drossart et al.*, 1989; *Maillard et al.*, 1990]. Such profiles also provide a correct fitting of the $CH_4$-$\nu_4$ band in the auroral region. Simultaneous observations of $H_2$, $H_3^+$, and hydrocarbons could therefore potentially provide a constraint on the thermal profile from the 100-μbar up to the 0.1-μbar levels.

An additional constraint on the thermal profiles is provided by the emissions due to the other hydrocarbon bands. The ratio of the emission excess in the other hydrocarbons to the emission excess in $CH_4$ is shown in Figure 5 as a function of the pressure level $P_s$. From Figure 5, it is possible to determine the value of $P_s$ that gives the best fit for both $CH_4$ and $C_2H_2$. Maximum contribution to the emission originates from around 20 μbar, as shown in Figure 6. We have thus produced thermal profiles which are consistent with our initial hypothesis that the excess emission originates in an altitude range where the hydrocarbon absorptions are still optically thin. The observed enhancement in $C_2H_6$ cannot be explained in this model. Due to the vertical profile of $C_2H_6$ in the "nominal" photochemical model and to the less intense band strength, the optical depth above $P_s$ is too low to produce enough excess emission in the auroral hot spot. Provided that our photochemical calculations are correct, we conclude that the thermal profile would also need to be slightly modified at deeper levels to account for the $C_2H_6$ excess emission. The main result is that $C_2H_2$ and $CH_4$ auroral excess emissions can be accounted for to a first order by our model, in which temperatures are enhanced at altitudes above the 100-μbar pressure level.

These conclusions are verified by complete line-by-line calculations, the results of which are presented, along with the

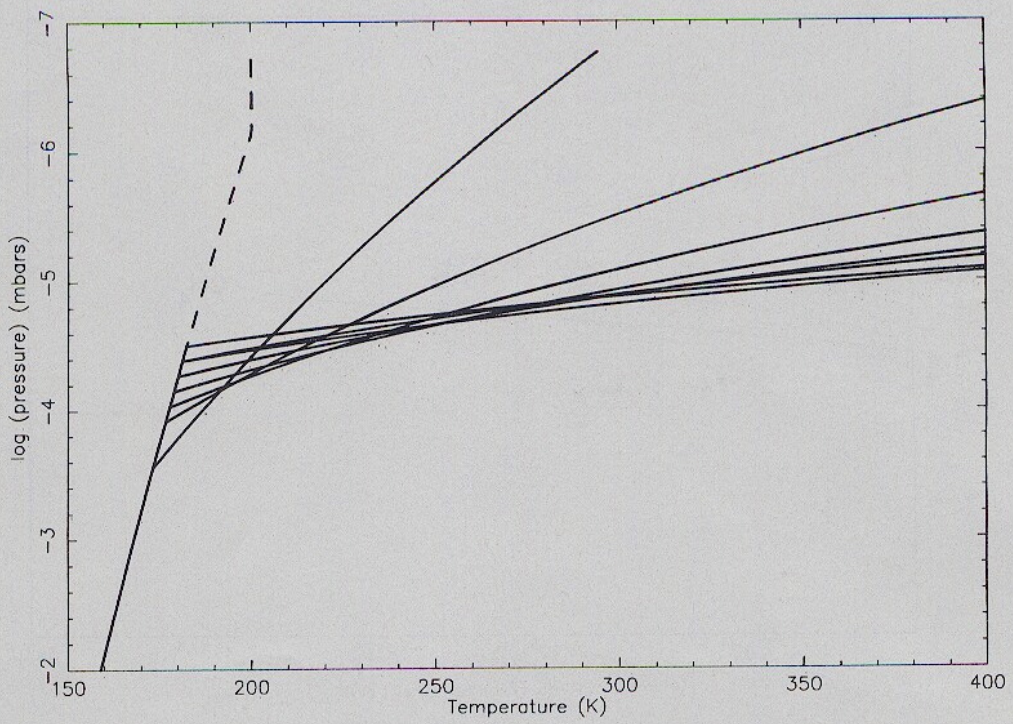


Fig. 4. Thermal profiles. Starting from a "nominal" thermal profile, and using the optically thin auroral model described in the text, all the thermal profiles in solid lines are calculated to fit the $CH_4$ excess auroral emission shown in Figure 2, with a constant lapse rate in the upper atmosphere. The profiles are characterized by the pressure $P_s$ at which they separate from the nominal thermal profile, and their (constant) lapse rate for $P \leq P_s$.

Voyager IRIS data, in Figure 7. These calculations include non-LTE effects and do not assume an optically thin emission layer; they therefore do not depend on the approximation made above for fast thermal profile calculations. By comparing this integrated emission within the $CH_4$ band to the emission calculated in the optically thin approximation described above, we can correct the thermal profile calculated above (by about 25%) to fit the $CH_4$ band. The final profile thus reproduces the auroral emission exactly, and the

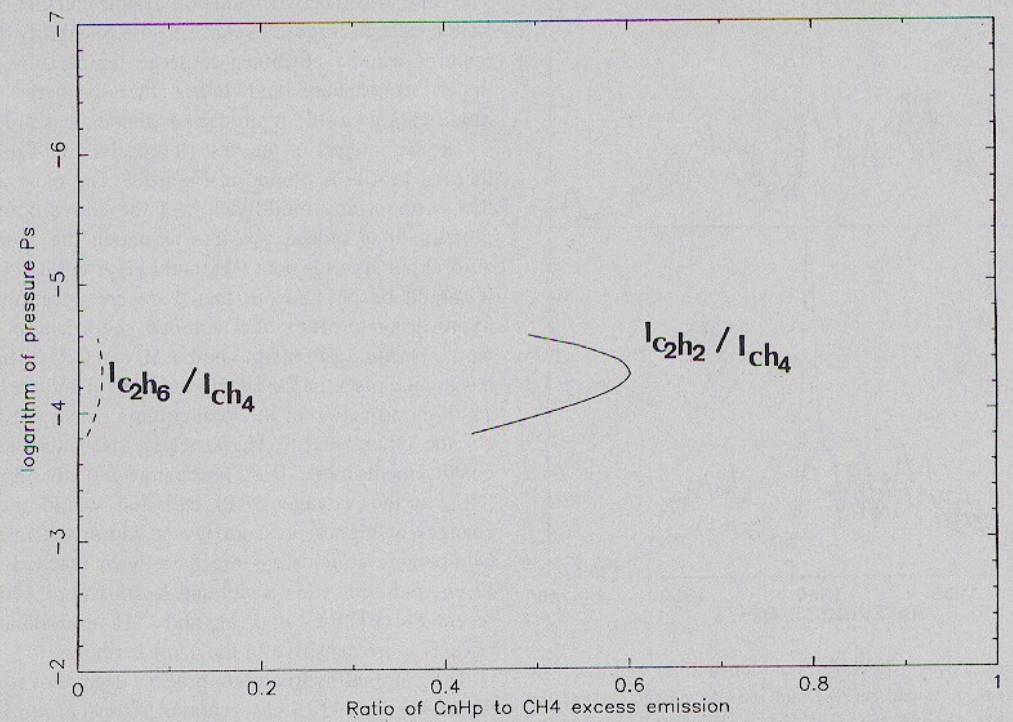


Fig. 5. Ratio of excess auroral emission in $C_2H_2$ to $CH_4$ (solid line) and of $C_2H_6$ to $CH_4$ (dashed line). For each auroral thermal profile in Figure 4, the ratio of excess emission in $C_2H_2$ to the excess emission in $CH_4$ (compared to the nominal profile) is plotted (solid line), versus the pressure $P_s$, above which the thermal profile has a constant lapse rate. Voyager/IRIS spectra yield a ratio of 0.92; the best fit is obtained for the maximum value of this ratio (0.68). The excess in $C_2H_6$ (dashed line) is comparatively much lower.

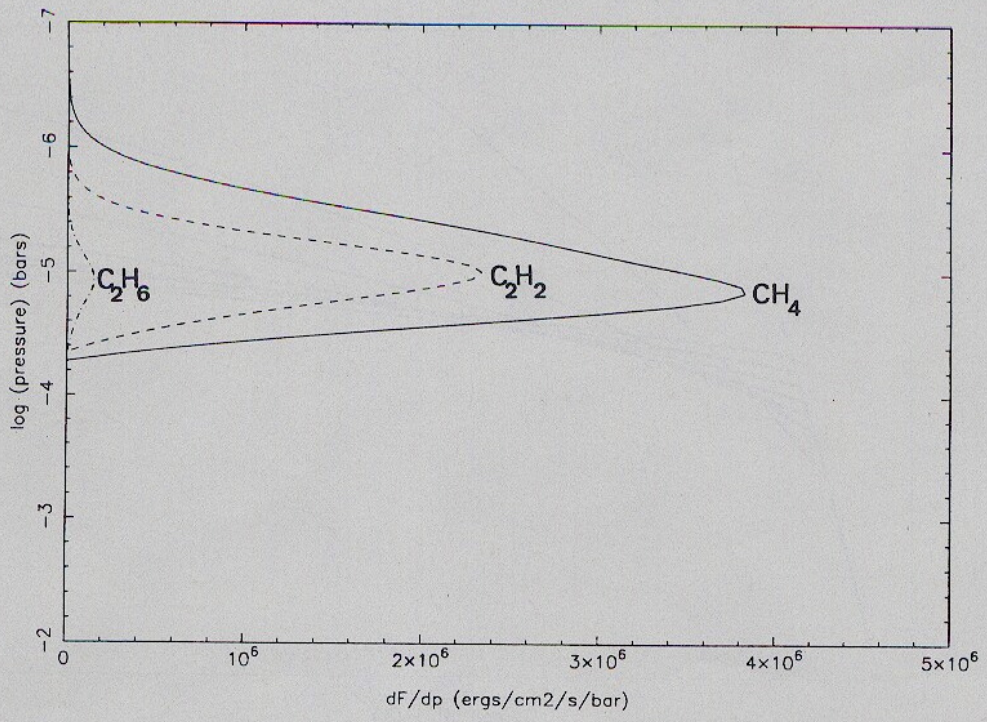


Fig. 6. Vertical variation of auroral emission for the best fit. The temperature profile used corresponds to the best fit found from the radiative transfer model. The vertical repartition of the auroral emission for the best profile determined from Figures 4 and 5 shows a strong maximum for $CH_4$ and $C_2H_2$ around 20 μbar.

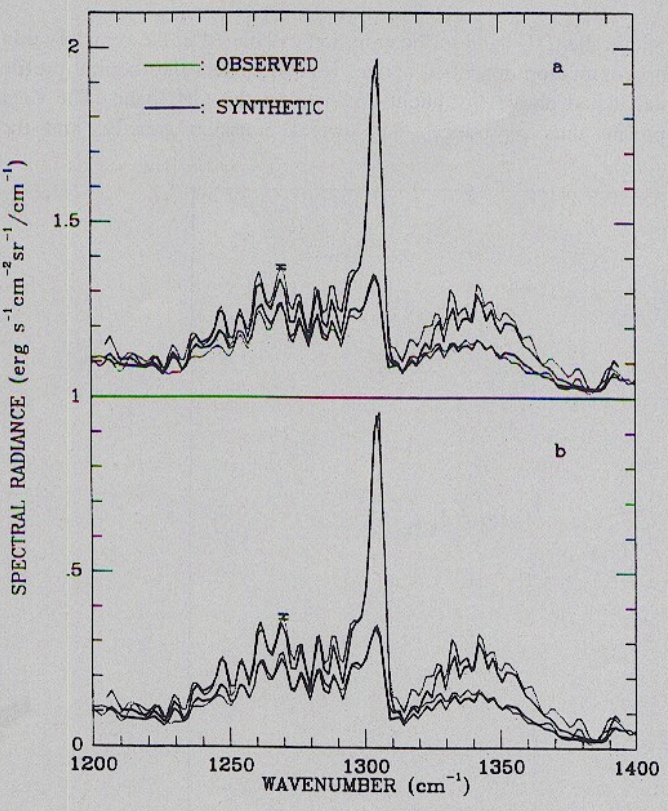


Fig. 7. Comparison of Voyager/IRIS spectra (dotted line) and synthetic spectra (solid line) within (upper curves) and outside (lower curves) the auroral hot spot, in the spectral range of $CH_4$-$\nu_4$ band. (a) Line-by-line calculations are performed for the parameters given in Table 2, and for the hydrocarbon profiles of *Atreya et al.* [1981], except for an adjustment for the $CH_4$ deep abundance, which has been multiplied by 1.3 to fit the most recent value of $CH_4$ abundance. (b) same as Figure 7*a* for the *Gladstone* [1982] profile, and the corresponding parameters of Table 2.

enhancement in $C_2H_2$ is only 25% too low (Figure 8). The $C_2H_6$ emission is almost unchanged. Moreover, a good fit is obtained in the P, Q, and R branches of $CH_4$, which gives an independent check of the consistency of our hypothesis, since the thermal profiles have been derived by fitting only the global emission in the full band. The comparison between the line-by-line calculations and the auroral IRIS spectrum (Figure 7) confirms the possibility that these emission features can be attributed to large temperature variations in the upper stratosphere and lower thermosphere; and only minor modifications in the hydrocarbon abundances are required.

The parameters of the best fit are given in Table 2, and the final thermal profile is plotted in Figure 9. The most important result is that, without any modification of the above nominal hydrocarbon profiles, it is indeed possible to match the observed flux in the auroral hot spot for both $CH_4$ and $C_2H_2$ (within 25%). Nevertheless, it should be pointed out that there are uncertainties in the exact hydrocarbon profiles, and a minor modification of these profiles would permit a better fit to both $CH_4$ and $C_2H_2$. The required change has to take place in the 10–50 μbar region and corresponds to a very small modification of the total column density of the hydrocarbons. On the other hand, $C_2H_6$ is nearly insensitive to the temperature enhancement in the 10–50 μbar range and any improvement in fit of $C_2H_6$ to the Voyager IRIS emission would require temperature changes at higher pressure levels within the middle stratosphere. Comparable conclusions are have been reached independently by *Livengood et al.* [this issue] and *Kostiuk et al.* [this issue] based on recent observations of $C_2H_6$ and $C_2H_4$ emissions; they show that $C_2H_6$ is more sensitive in the 1-mbar region.

The nominal hydrocarbon profiles used above were calculated to fit the Voyager UVS observations [*Atreya et al.*, 1981]. Since these profiles fit observations recorded nearly simultaneously with the Voyager IRIS observations, we have incorporated them in our nominal model. However, uncertainties in the chemical kinetics and possible pathways could result in uncertainties in model results. We have therefore performed infrared synthetic spectra calculations

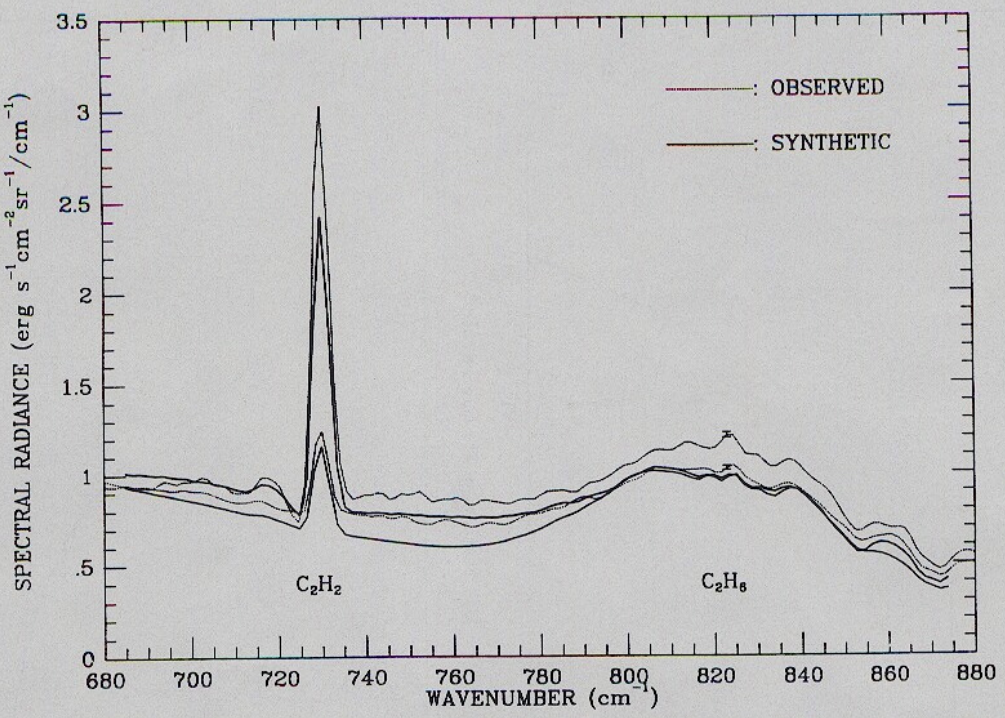


Fig. 8. Comparison of Voyager/IRIS spectra (dotted line) and synthetic spectra (solid line) within (upper curves) and outside (lower curves) the auroral hot spot in the region of $C_2H_2$ and $C_2H_6$ emissions. Line-by-line calculations for the parameters given in Table 2 and for the hydrocarbon profiles of *Atreya et al.* [1981]. The abundance of $C_2H_2$ has been multiplied by 1.3 to fit the Q branch.

using the hydrocarbon profiles of *Gladstone* [1982], which are also close to the profiles fitting some IUE observations [*Gladstone and Skinner*, 1989]. The main difference between these profiles and those in the model of *Atreya et al.* [1981] is that $CH_4$ is more abundant by a factor of 10 in the model of *Gladstone* [1982] at pressures less than 10 μbar. Unfortunately, model calculations in this region are not constrained by observations. The same radiative transfer model is applied, and the resulting temperature profiles are presented in Figure 9, for comparison with the profile obtained from the "nominal model"; the parameters of the fit are also given in Table 2. As expected, the large temperature gradient takes place at higher altitudes, but the main conclusions are still valid. Synthetic calculations in the $\nu_4$ band of $CH_4$ for both profiles are presented for comparison to Voyager IRIS observations (Figure 7a and 7b). Table 2 gives the results for the excess energy in each hydrocarbon.

## Implications of Infrared Emissions for Auroral Energetics

The total energy flux enhancement calculated from the excess emissions observed by Voyager/IRIS is 208 ergs cm$^{-2}$ s$^{-1}$. This is much greater than that usually inferred from the UV auroral emissions [*Waite et al.*, 1983]. The difference between the energy flux estimated from the ultraviolet spectrometer (UVS) data (10 ergs cm$^{-2}$ s$^{-1}$) and the IRIS value (208 ergs cm$^{-2}$ s$^{-1}$) can be accounted for by differences in the assumed emissions areas. More precisely, recent Hubble space telescope/faint object camera observations indicate that the size of the auroral hot spot may be less than 1000 by 1000 km, compared to the size assumed in the Voyager UVS data (≈6,000 × 40,000 km [*Herbert et al.*, 1987]). This would imply concentrated emission features of more than 200 kR with resulting energy fluxes of more than 20 ergs cm$^{-2}$ s$^{-1}$ and a power of about $10^{13}$ W [*Dols et al.*, 1992]. Nevertheless, the magnitude of the energy difference between the UV and IR emissions suggests that Joule heating might play a significant role in auroral heating as an additional source of energy.

TABLE 2. Results for the Hydrocarbon Excess Emission

| | $I(C_2H_2)/I(CH_4)$ | $I(C_2H_6)/I(CH_4)$ |
|---|---|---|
| Observed | 0.92±0.10 | 0.28±0.15 |
| Calculated* | 0.72 | 0.02 |
| Calculated† | 0.67 | 0.03 |

*Hydrocarbon profile from *Atreya et al.* [1981], $P_s$ = 74 μbar, $dT/dz$ = 1.7 K km$^{-1}$.

†Hydrocarbon profile from *Gladstone*, [1982], $P_s$ = 35 μbar, $dT/dz$ = 1.23 K km$^{-1}$.

By multiplying the excess emission area of the IRIS field of view, the total amount of energy radiated to space by the hydrocarbon emissions is found to be about 4 × $10^{13}$ W. This amount, which corresponds only to the auroral hot spot, is, however, relatively consistent with the energy influx from particle precipitation inferred from Voyager UVS observations. The results of *Herbert et al.* [1987] indicate that 20 to 30% of the emission comes from the auroral hot spot. Further, their estimates of the emitted power at UV wavelengths (in their Table 2) can be combined with the emission efficiencies given by *Waite et al.* [1983] to estimate the input power. The total auroral power input thus estimated is 1.2 × $10^{14}$ W for Voyager 1 inbound and 4 × $10^{13}$ W for Voyager outbound. These values are to be compared with the *Livengood et al.* [1990] average values from 10 years of International Ultraviolet Explorer (IUE) data of 2.4 × $10^{13}$ W with a 1-σ variance of ≈1 × $10^{13}$ W and variations of up to a factor of 6 over the span of less than one month. Combining the Voyager UVS and IUE observations therefore suggests that the power input into the auroral hot spot ranges from 5 × $10^{12}$ to 4 × $10^{13}$ W. Further, if a 50% heating efficiency is assumed [*Waite et al.*, 1983], then the expected infrared emission from particle precipitation sources ranges from 3 × $10^{12}$ to 2 × $10^{13}$ W. These estimates of auroral power from particle precipitation (as defined by the UV observations) thus leave

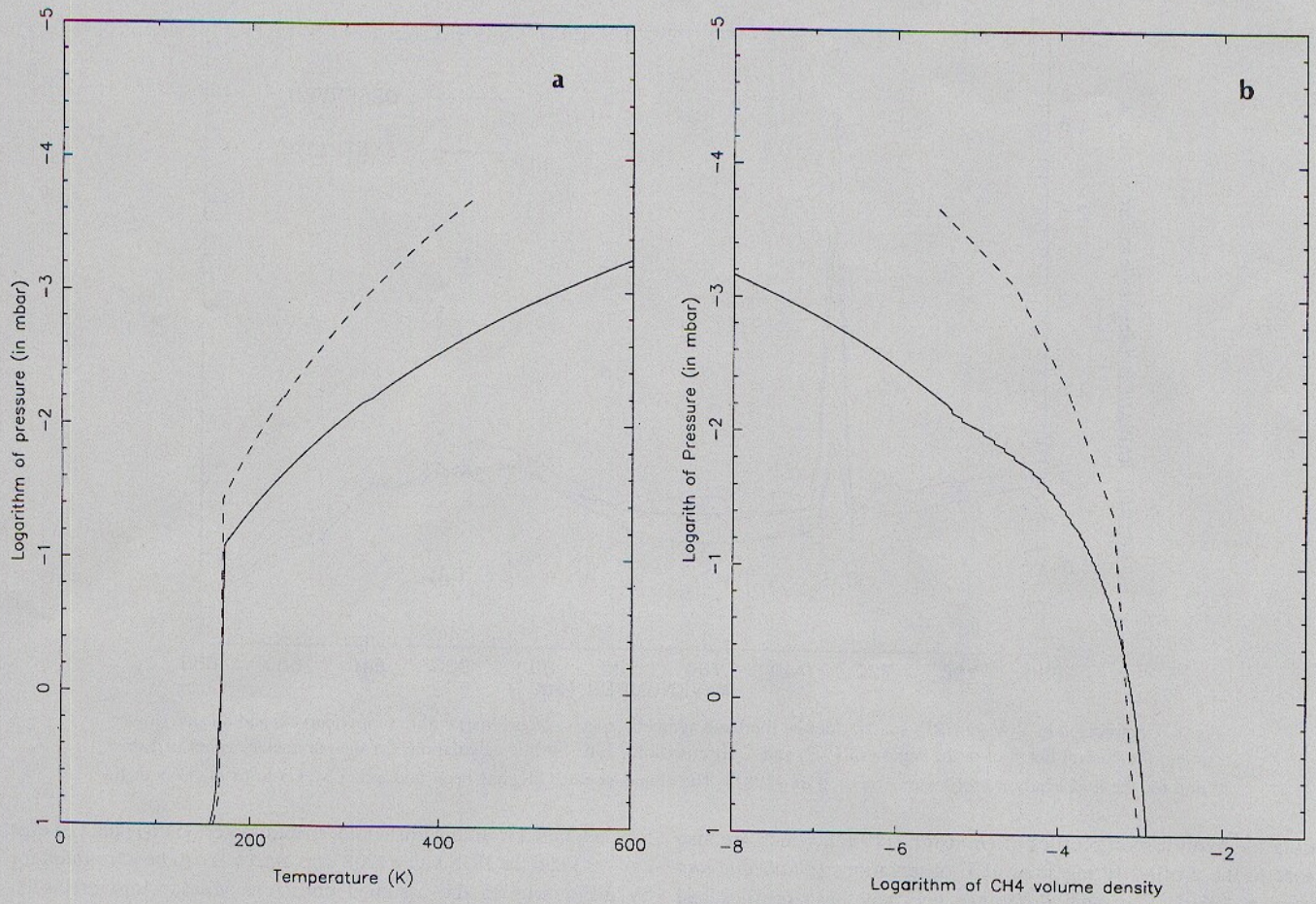


Fig. 9. (a) Thermal profiles corresponding to the best fit for hydrocarbon emissions, for the hydrocarbon distribution of *Atreya et al.* [1981] (solid curve) and for the hydrocarbon distribution of *Gladstone* [1982] (dashed curve). (b) $CH_4$ abundance for the hydrocarbon distribution of *Atreya et al.* [1981] (solid curves) and for the hydrocarbon distribution of *Gladstone* [1982] (dashed curve).

open the relative role of Joule heating in the auroral zone. However, reasonable scaling arguments would imply that over 50% of the infrared emission may result from Joule heating. In addition, Joule heating has been proposed to occur in the auroral region in many models [e.g., *Waite et al.*, 1983] and was also suggested by *Zhan and Dessler* [1990] as a possible explanation for the South auroral hot spot drift.

Using a combination of in situ satellite data and thermospheric general circulation model (TGCM) modeling techniques, *Roble et al.* [1987] have shown that localized Joule heating in the Earth's lower thermosphere can exceed 400 ergs $cm^{-2}$ $s^{-1}$. It is conceivable that Joule heating of at least the same magnitude could occur in Jupiter's thermosphere. *Nishida and Watanabe* [1981] have estimated the Joule heating from Iogenic mass loading and from expansion and contraction of the Jovian magnetosphere via the solar wind. Using an assumed value of 0.1 mho for the integrated Pedersen conductivity, they obtain heating rates that range from 10 to greater than 100 ergs $cm^{-2}$ $s^{-1}$. However, local precipitation of energetic particles may significantly increase the ionospheric conductivity, producing changes of over two orders of magnitude [*Waite et al.*, 1983]. This, however, may be partially compensated by slippage of the neutral atmosphere, which reduces the effective Pedersen conductivity [*Huang and Hill*, 1989]. In balance, a net increase in the Pedersen conductivity within localized precipitation regions by a factor of 3 to 20 is not inconceivable. Based on the early results of Nishida and Watanabe [1981], we conclude that such increases in the conductivity would easily produce heating rates greater than 200 ergs $cm^{-2}$ $s^{-1}$. In light of this new analysis, detailed calculations of the conductivity enhancements should be carried out.

## CONCLUSIONS

This model shows that it is possible to achieve a reasonably good fit between modeled and observed auroral zone hydrocarbon emissions by adjusting the thermal gradient in the upper stratosphere; only a small change in the hydrocarbon abundances is necessary. This contradicts the conclusions of previous authors, which require the thermal profile to be modified down to the 1-mbar region, where emission from hydrocarbon bands is optically thick [*Kim et al.*, 1985; *Kostiuk et al.*, 1989]. Here, the temperature modifications take place only at pressures of around 50 μbar, the most sensitive pressure level being between 10 and 20 μbar depending on the hydrocarbon profile. The nominal hydrocarbon profile used in our model does not yield an exact reproduction of the observed hydrocarbon emission. This may be due to uncertainties in the photochemical scheme or reaction rates used in the photochemical model or to a modification of the chemistry within the auroral zone. However, the modification required to fit the $C_2H_2$ emission would be much smaller than assumed in the previous models, since the variation of column density required to fit $C_2H_2$ is only of a few $10^{-3}$ compared to the column density down to 1 mbar. Such modifications could in fact be the result of

electrochemistry induced by magnetospheric charged particles cascading through the upper atmosphere.

The main paradox in the present work is how to explain the amount of energy required to balance the infrared emission, which seems too large to be only due to auroral particle precipitation. We suggest that part of this energy could come from enhanced Joule heating in the same altitude range. A self-consistent model of the radiatively controlled atmosphere will be constructed later to test this hypothesis.

*Acknowledgements.* Research by S.K.A. and J.H.W. was supported by a grant from the Planetary Atmospheres Program of the NASA Solar System Exploration Division.

## REFERENCES

Appleby, J. F., $CH_4$ nonlocal thermodynamic equilibrium in the atmospheres of the giant planets, *Icarus*, *85*, 355-379, 1990.

Atreya, S. K., T. M. Donahue, and M. C. Festou, Jupiter: structure and composition of the upper atmosphere, *Astrophys. J.*, *247*, L43–L47, 1981.

Bishop, J., S. K. Atreya, P. R. Romani, B. R. Sandel, and F. Herbert, Voyager 2 ultraviolet spectrometer solar occultation at Neptune: Constraints on the abundance of methane in the stratosphere, *J. Geophys. Res.*, *97*, 11,681–11,694, 1992.

Caldwell, J., A. T. Tokunaga, and F. C. Gillett, Possible infrared aurorae on Jupiter, *Icarus*, *44*, 667–675, 1980.

Caldwell, J., R. Halthore, G. Orton, and J. Bergstralh, Infrared polar brightenings on Jupiter, IV, Spatial properties of methane emission, *Icarus*, *74*, 331–339, 1988.

Dols, V., J. C. Gérard, F. Paresce, R. Prangé and A. Vidal-Madjar, Ultraviolet imaging of the Jovian aurora with the Hubble space telescope, *Geophys. Res. Lett.*, *19*, 1803–1806, 1992.

Drossart, P., E. Serabyn, J. Lacy, S. Atreya, B. Bézard, and T. Encrenaz, Acetylene, ethane and polar infrared brightening on Jupiter (abstract), *Bull. Am. Astron. Soc.*, *17*, 708, 1985.

Drossart, P., B. Bézard, S. Atreya, J. Lacy, E. Serabyn, A. Tokunaga, and T. Encrenaz, Enhanced acetylene emission near the north pole of Jupiter, *Icarus*, *66*, 610–618, 1986.

Drossart, P., et al., Detection of $H_3^+$ on Jupiter, *Nature*, *340*, 539–541, 1989.

Gladstone, G. R., Radiative transfer and photochemistry in the upper atmosphere of Jupiter, thesis, Calif. inst. of Technol., Pasadena, 1982.

Gladstone, G. R., and T. E. Skinner, Spectral analysis of Jovian auroral emissions, in Time-variable phenomena in the Jovian system, *NASA Spec. Publ.*, *SP494*, 221–228, 1989

Halthore, R., A. Burrows, and J. Caldwell, Infrared brightenings on Jupiter, V. A thermal equilibrium model for the north polar hot spot. *Icarus*, *74*, 340–350, 1988.

Hanel, R., et al., Infrared observations of the Jovian system with Voyager 1, *Science*, *204*, 972–976, 1979.

Herbert, F., B.R. Sandel, and A. L. Broadfoot, Observations of the Jovian UV aurora by Voyager, *J. Geophys. Res.*, *92A*, 3141–3154, 1987.

Houghton, J. T., *The Physics of Atmospheres*, Cambridge University Press, New York, 1986.

Huang, T., and T. Hill, Corotation tag of the Jovian atmosphere, ionosphere, and magnetosphere, *J. Geophys. Res.*, *94A*, 3761–3765, 1989.

Husson, N. et al., The GEISA spectroscopic line parameters data bank in 1984, *Ann. Geophys.*, *4*, 185–190, 1986.

Kim, S. J., J. Caldwell, A. R. Rivolo, and R. Wagener, Infrared polar brightening on Jupiter, III, Spectrometry from Voyager IRIS experiment, *Icarus*, *64*, 233-248, 1985.

Kim, S. J., P. Drossart, J. Caldwell, and J.-P. Maillard, Temperatures of the Jovian auroral zone inferred from 2 μm $H_2$ quadrupole line observations, *Icarus*, *84*, 54–61, 1990.

Kim, Y. H., J.L. Fox, and H. S. Porter, Densities and vibrational distribution of $H_3^+$ in the jovian auroral ionosphere, *J. Geophys. Res.*, *97*, 6093–6101, 1992.

Kostiuk, T., F. Espenak, M. J. Mumma, D. Deming, and D. Zipoy, Variability of ethane on Jupiter, *Icarus*, *72*, 384–410, 1987.

Kostiuk, T., F. Espenak and M. J. Mumma, Is ethane varying in the Jovian north polar "hot spot," in Time-variable phenomena in the Jovian system, *NASA Spec. Publ.*, *SP494*, 234–241, 1989.

Kostiuk, T., P. Romani, F. Espenak, T. Livengood, and J. Goldstein, Temperature and abundances in the Jovian auroral stratosphere, 2, Ethylene as a probe of the microbar region, *J. Geophys. Res.*, this issue.

Livengood, T. A., D. F. Strobel, and H. W. Moos, Long-term study of longitudinal dependence in primary particle precipitation in the north Jovian aurora, *J. Geophys. Res.*, *95*, 10,375–10,388, 1990.

Livengood, T. A., T. Kostiuk, F. Espanak, and J. Goldstein, Temperatures and abundances in the Jovian auroral stratosphere,1, Ethane as a probe of the millibar region, *J. Geophys. Res.*, this issue.

Maillard, J.-P., P. Drossart, J. K. G. Watson, S. J. Kim, and J. Caldwell, $H_3^+$ fundamental band in Jupiter auroral zones at high resolution from 2400 to 2900 inverse centimeters, *Astrophys. J.*, *363*, L37–L41, 1990.

Nishida, A., and Y. Watanabe, Joule heating of the Jovian ionosphere by corotation enforcement currents, *J. Geophys. Res.*, *86*, 9945–9952, 1981.

Roble, R. G., et al., Joule heating in the mesosphere and thermosphere during the July 13, 1982, solar proton event, *J. Geophys. Res.*,92, 6083–6090, 1987.

Waite J. H. Jr, T. E. Cravens, J. U. Kozyra, A. F. Nagy, S. K. Atreya, and R. H. Chen, Electron precipitation and related aeronomy of the Jovian thermosphere and ionosphere, *J. Geophys. Res.*, *88*, 6143–6163, 1983.

Wallace, L., Stratosphere and upper troposphere, in *Jupiter*, edited by T. Gehrels, pp. 284–303, University of Arizona Press, Tucson, 1976.

Zhan, J. and A. J. Dessler, A magnetospheric model of the Jovian north and south polar infrared hot spot, paper presented at Symposium on Magnetospheres of the Outer Planets, Am. Astron. Soc., Annapolis, Md., 1990.

S. K. Atreya and J. Bishop, Department of Atmospheric, Oceanic and Space Sciences, University of Michigan, Ann Arbor, MI 48109-2143.

B. Bézard and P. Drossart, Centre National de la Recherche Scientifique, Départment Spatial, Observatorie de Paris-Meudon, France.

D. Boice and J. H. Waite, Jr., Department of Space Science, Southwest Research Institute, San Antonio, TX 78228-0510.

(Received October 2, 1992;
revised June 11, 1993;
accepted July 2, 1993.)